

Origin of the ESR linewidth in the normal phase of $\text{GdBa}_2\text{Cu}_3\text{O}_7$

A. Deville, L. Bejjit, B. Gaillard, and J. P. Sorbier

*Laboratoire d'Electronique des Milieux Condensés, Université de Provence, Centre St.-Jérôme,
13397 Marseille CEDEX 13, France*

O. Monnereau

Laboratoire de Chimie des Matériaux, Université de Provence, Centre St.-Charles, 13331, Marseille CEDEX 3, France

H. Noel and M. Potel

*Laboratoire de Chimie du Solide et Inorganique Moléculaire, Université de Rennes, Avenue Général Leclerc,
35042 Rennes CEDEX, France*

(Received 23 April 1992)

The ESR linewidth of the superconducting oxide $\text{GdBa}_2\text{Cu}_3\text{O}_7$ in the normal state is studied experimentally at 300 K. Several factors that strongly affect its shape and width—skin effect, contribution of the ω_- resonance, and chemical preparation—are examined carefully, and in this context some experimental results on Gd_2O_3 are presented. It is shown that Q -band spectra from both $\text{GdBa}_2\text{Cu}_3\text{O}_7$ powders (Lorentzian line) and single crystals (isotropic spectra) are of particular interest for theoretical analysis. The g factor of Gd^{3+} in $\text{GdBa}_2\text{Cu}_3\text{O}_7$ is found to be 2.01 ± 0.01 . Experimental results are given that indicate the existence of an exchange-narrowed dipolar line, via the Van Vleck–Anderson mechanism and not the Plefka-Barnes mechanism. Both the second moment of the ESR dipolar line, and the contribution of exchange to the fourth moment for a powder and for selected field orientations in the case of a single crystal are calculated numerically. Comparison of the predictions of the Van Vleck–Anderson–Weiss model with experimental results suggests that the nonadiabatic situation is present even at the Q band, and the coupling constant between nearest neighbors is found to be $2J/k = -0.3$ K. Finally, the effect of the coupling with the conduction electrons is discussed, and an experimental check is made in a dilute sample.

I. INTRODUCTION

The mechanism of superconductivity in high-temperature superconductors (HTSC) is not identified yet. One suggestion is that the antiferromagnetic (AF) couplings could play a decisive role.^{1–3} In this context the interest of studying the magnetic couplings with ESR is clear. We have previously studied $\text{YBa}_2\text{Cu}_3\text{O}_7$. It has been suggested⁴ and confirmed by single-crystal studies^{5,6} that the Cu^{2+} ion is not detected by ESR at 300 K in this material, and that the possible ESR signal comes from traces of a spurious phase, the green phase.^{5,7} It was then natural to try and get information on the magnetic couplings replacing the nonmagnetic Y^{3+} ion by a magnetic ion, and an ideal candidate is Gd^{3+} (no charge compensation, $L=0$). There is a second reason for the study of the magnetic properties of $\text{GdBa}_2\text{Cu}_3\text{O}_7$. The Abrikosov-Gorkov theory⁸ indicates that introducing a small proportion of magnetic impurities induces a strong decrease of T_c , and possibly a suppression of superconductivity. However, $\text{GdBa}_2\text{Cu}_3\text{O}_7$ has the same T_c (90 K) as $\text{YBa}_2\text{Cu}_3\text{O}_7$, and an explanation has to be found. This behavior could, for instance, be related to an absence of strong coupling between the Gd^{3+} ions and the conduction electrons, or linked to a suggestion made by De Gennes,¹ and more experimental data are necessary for the answer to be unambiguously established.

In this paper, the ESR line in the normal state is examined experimentally, at 300 K, and theoretically. The experimental line from both single crystals and sintered samples is found to be quite asymmetrical. We show that this is so because the skin effect is present (X and Q bands) and the ESR line is broad, i.e., its width is comparable with the resonance field (X band). The ESR linewidth is, moreover, found to depend on chemical preparation, contrary to what could be presupposed. The published literature clearly leads to this conclusion. Excluding the results from Schwartz,⁹ obviously obscured by the presence of an intense and wide undesirable signal from some impurity or unwanted phase, we note that Nakamura¹⁰ obtained a peak-to-peak width $\Delta B_{pp} = 270$ mT with both superconducting ($T_c \approx 90$ K) and nonsuperconducting samples, which compares favorably with results from Kikuchi:¹¹ $\Delta B_{pp} = 250$ mT ($T_c \approx 91$ K) and 280 mT (nonsuperconducting sample), while on the contrary Mehran¹² found $\Delta B_{pp} \approx 100$ mT ($T_c \approx 90$ K), none of these results being from single crystals. We did observe similar strong differences between samples prepared differently:¹³ $\Delta B_{pp} = 280$ mT (sintered samples) and $\Delta B_{pp} = 110$ mT (single crystals prepared by a mineralization process, the width was then unchanged after grinding).

The samples—sintered samples (preparation A) and single crystals prepared either by the mineralization pro-

cess (preparation *B*) or by the flux method (preparation *C*)—and the experimental method are presented in Sec. II. The experimental results are given in Sec. III, together with the fits with analytical expressions intended to describe the skin effect and/or the presence of the ω_- resonance. The effect of grinding, that of removing oxygen through annealing, and results upon the ESR of Gd^{3+} in Gd_2O_3 are also presented. The theoretical determination of the dipolar linewidth and of the effect of exchange is given in Sec. IV.

II. SAMPLES AND EXPERIMENTAL CONDITIONS

The samples from preparation *A*—sintered samples—were obtained from a stoichiometric mixture of CuO , Gd_2O_3 , and BaCO_3 powders. This mixture underwent several heat treatments (950°C , air) separated by grinding, then an oxygenation (960°C , 24 h) and a slow cooling down to room temperature (RT), in an alumina crucible. The resulting material was a brittle solid. The x-ray-diffraction spectra could be indexed assuming orthorhombic structure and $a=3.8369\pm 0.0033$ Å, $b=3.8963\pm 0.0037$ Å, $c=11.6881\pm 0.0086$ Å, which is in agreement with known results upon $\text{GdBa}_2\text{Cu}_3\text{O}_7$.^{14,15} The thermal variation of the low-frequency resistivity of a sample from preparation *A* is given in Fig. 1. The existence of the SC transition for the different samples was checked directly by observing the change of the reflection coefficient of the cavity at T_c (contactless measurement). The single crystals were grown by a mineralization process (preparation *B*) already described^{5,7} or by the flux method (preparation *C*). All $\text{GdBa}_2\text{Cu}_3\text{O}_7$ samples for which ESR results are given were superconducting, with T_c between 88 and 91 K. After annealing, the samples are designated as $\text{GdBa}_2\text{Cu}_3\text{O}_{7-\delta}$, and their superconductivity was lowered or suppressed (i.e., $T_c < 4$ K). ESR measurements at the *X* band (9.3 GHz) were done with a Bruker ESR 300 spectrometer, using a gas-flow cryostat (Oxford ESR 9) and the Varian rectangular dual cavity (TE_{104}). The *Q*-band measurements (35 GHz) were done with the Varian E110 bridge and a cylindrical cavity, and with a gas-flow cryostat (Oxford CF 35). The single crystals were stuck at the end of a silica capillary tube. The other samples were put into a silica ESR tube.

III. EXPERIMENTAL RESULTS

We will call H the static field in ESR experiments. In the theoretical discussion we will use SI units. We therefore use $B = \mu_0 H$ both in this discussion and in the pre-

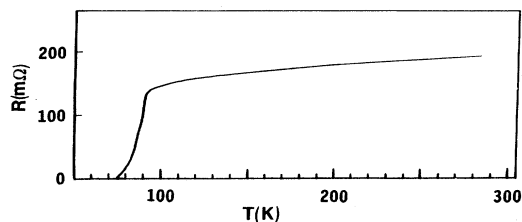


FIG. 1. Thermal dependence of the low-frequency resistance for a $\text{GdBa}_2\text{Cu}_3\text{O}_7$ sintered sample.

sentation of the experimental ESR results. In this presentation, in addition to the A/B ratio, which measures the asymmetry of the line, we have systematically indicated the experimental results, $g_{\text{eff}} = h\nu/\beta B$ (β is the Bohr magneton), and ΔB_{pp} , the experimental peak-to-peak linewidth. Even if they presently have generally no direct physical meaning, they allow easy comparison with other experimental results and are often given in the existing literature on ESR in superconductors (c.f. Refs. 16–17). We have, moreover, tried to determine the intrinsic parameters: g factor, and $\Delta B_{i,\text{pp}}$, the peak-to-peak intrinsic linewidth, i.e., width in the absence of complications such as (1) skin effect, (2) presence of the wing of the ω_- resonance when $\Delta B_{i,\text{pp}} \approx$ resonance field, a consequence of the linear polarization of the rf field, when either seemed of interest. Two facts were quite helpful in the interpretation of the ESR spectra: measurements at the *Q* band besides those at the *X* band, and comparison of the spectra before and after grinding. We first present the results obtained with the single crystals from preparation *B*, which are simpler than those from the sintered samples.

The ESR spectra from a single crystal from preparation *B* are shown in Figs. 2, 3, curve *a* (*X* band), and 4, curve *a* (*Q* band). We first comment about the *X*-band spectrum. This spectrum is nearly isotropic (Fig. 2, and the fact that the spectrum is independent of a rotation of the static field around the c axis) and quite asymmetrical [Fig. 3, curve *a*, $A/B \approx 2.6$]. The apparent values are $g_{\text{eff}} \approx 1.82$ and $\Delta B_{\text{pp}} \approx 128 \pm 6$ mT (Fig. 3, curve *a*). The spectrum is approximately described with a Dysonian shape. Calling B_0 the resonance field for the Lorentzian line, $\Delta B = \sqrt{3}\Delta B_{i,\text{pp}}$, the width between half-height points of the Lorentzian line, and introducing $x = B/B_0$, $a = 2B_0/\Delta B$, and $U = a(x-1)$, then the theoretical expression $y' = (1-2U-U^2)/(1+U^2)^2$ is asymmetrical, with $A/B \approx 2.55$. A fit is obtained between this expression and experimental results using the following values for the Lorentzian line describing the absorption: $g = 2.046$ and $\Delta B_{i,\text{pp}} = 115$ mT. Some theoretical y' values obtained this way are reported in Fig. 3, curve *a*.

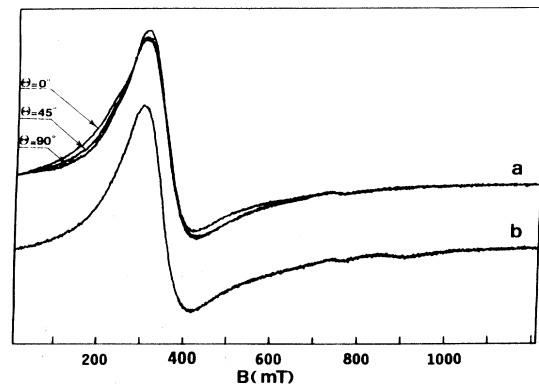


FIG. 2. *X*-band ESR spectrum from a $\text{GdBa}_2\text{Cu}_3\text{O}_7$ single crystal prepared by the mineralization process ($T=300$ K, $\nu=9384$ MHz, $P=20$ mW, and $B_{\text{mod}}=2$ mT_{pp}). (a) static field and c both horizontal, θ is the angle between c and the static field; and (b) static field in the ab plane.

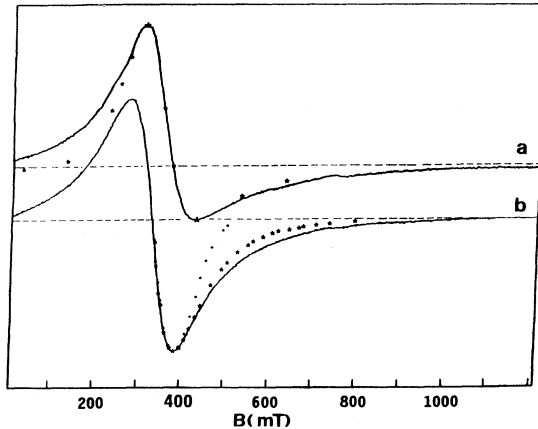


FIG. 3. X-band ESR spectra at $T=300$ K. (a) single crystal (mineralization). Static field $\parallel c$, $\nu=9384$ MHz, $P=20$ mW, and $B_{\text{mod}}=2$ mT. $g_{\text{eff}}=1.82$ and $\Delta B_{\text{pp}}=128\pm 6$ mT. Theoretical values using a Dysonian shape with $g=2.046$ and $\Delta B_{i,\text{pp}}=115$ mT are indicated by *. (b) powder sample [crystal in curve a is ground]. $\nu=9380$ MHz, $P=20$ mW, and $B_{\text{mod}}=2$ mT. $g=2.02$ and $\Delta B_{\text{pp}}=112\pm 6$ mT. Theoretical lines are given for a Lorentzian (*) and a Gaussian (●) shape. The intensity for the same mass of the sample is increased by a factor of 7.

The corresponding Q-band spectrum (Fig. 4, curve a) is also asymmetrical and isotropic ($g_{\text{eff}}\approx 1.96$, $\Delta B_{\text{pp}}\approx 124\pm 8$ mT), and is well described with a Dysonian shape, with $g=2.022$ and $\Delta B_{i,\text{pp}}=113$ mT. After grinding, the line recorded at the X band is [Fig. 3, curve b] nearly symmetrical ($A/B\approx 0.9$), with $g=2.02$ and $\Delta B_{\text{pp}}=112\pm 6$ mT. For the same mass of sample its intensity is increased by a factor of 7 by this grinding. The Q-band spectrum after grinding is given in Fig. 4, curve b. It is symmetrical ($A/B=1.01\pm 0.05$), with $g=2.004$

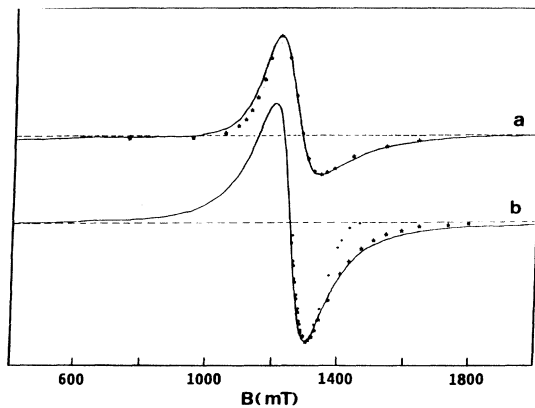


FIG. 4. Q-band ESR spectra at 300 K. (a) single crystal (same as in Fig. 3). Static field $\parallel c$, $\nu=34\,982$ MHz, $P=5$ mW, and $B_{\text{mod}}=4$ mT. $g_{\text{eff}}=1.96$ and $\Delta B_{\text{pp}}=124\pm 8$ mT. Theoretical values using a Dysonian shape with $g=2.022$ and $\Delta B_{i,\text{pp}}=113$ mT are indicated by (*). (b) powder sample (crystal in curve a is ground). $\nu=35\,001$ MHz, $P=5$ mW, and $B_{\text{mod}}=4$ mT. $g=2.004$ and $\Delta B_{\text{pp}}=108\pm 4$ mT. The intensity for the same mass of the sample is increased by a factor of about 20 by grinding. Theoretical values are given for a Lorentzian (*) and for a Gaussian (●) shape.

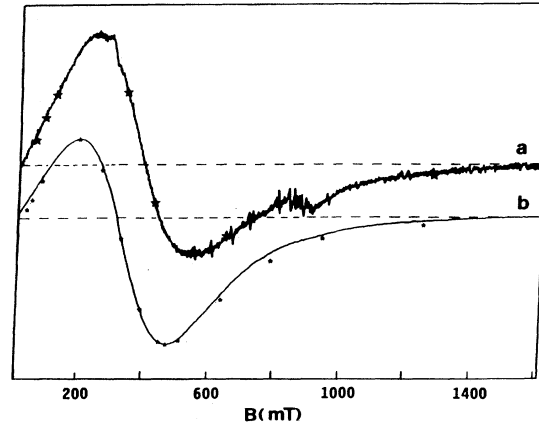


FIG. 5. X-band ESR spectra at $T=300$ K. (a) sintered sample. $\nu=9383$ MHz, $P=100$ mW, $B_{\text{mod}}=2$ mT. $A/B\approx 1.45$, $g_{\text{eff}}=1.70$, and $\Delta B_{\text{pp}}=302$ mT. The spectrum can be fitted (*) by taking account of both the presence of χ' , with an unusual proportion, and the presence of the ω_- resonance, with $g=2.013$ and $\Delta B_{i,\text{pp}}=307$ mT (see text). (b) powder sample (sintered sample in curve a is ground). $\nu=9380$ MHz, $P=20$ mW, and $B_{\text{mod}}=2$ mT. The signal is still asymmetrical, but with $A/B < 1$ ($A/B=0.62$, $g_{\text{eff}}=2.13\pm 0.02$, $\Delta B_{\text{pp}}=281\pm 8$ mT). It can be described (*) by taking into account the presence of the ω_- resonance, with $g=2.037$, $\Delta B_{i,\text{pp}}=304\pm 10$ mT (see text).

and $\Delta B_{\text{pp}}=108\pm 4$ mT. The factor for the intensity increase is now 20 rather than 7.

The spectra from a sintered sample are presented in Figs. 5, curve a (X band) and 6, curve a (Q band). The X-band spectrum obtained then (Fig. 5, curve a) is the most complex of all those presented in this paper. It is asymmetrical with A/B far less than 2.55 ($A/B\approx 1.45$), $g_{\text{eff}}=1.70$, and $\Delta B_{\text{pp}}=302$ mT. The corresponding Q-

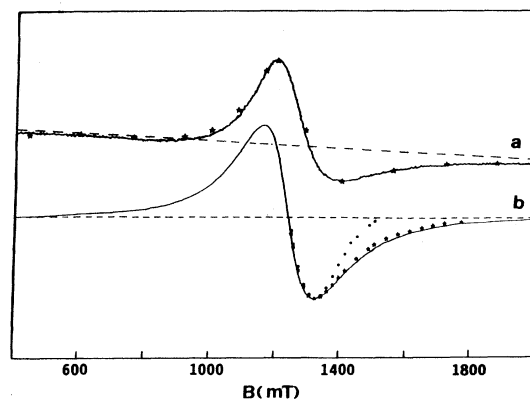


FIG. 6. Q-band ESR spectra at $T=300$ K. (a) sintered sample (same as in Fig. 5). $\nu=34\,831$ MHz, $P=5$ mW, and $B_{\text{mod}}=4$ mT. $g_{\text{eff}}=1.92$, $\Delta B_{\text{pp}}=202\pm 8$ mT. The line can be fitted (*) using a Dysonian shape with $g=2.013$ and $\Delta B_{i,\text{pp}}=178\pm 8$ mT, and an additional drift term. (b) powder sample (sintered sample as in curve a is ground). $\nu=34\,792$ MHz, $P=5$ mW, $B_{\text{mod}}=4$ mT. The spectrum is symmetrical, with $g=2.01$ and $\Delta B_{\text{pp}}=170\pm 4$ mT. Theoretical values are given for a Lorentzian (*) and a Gaussian (●) shape.

band spectrum is also asymmetrical, but now with $A/B \approx 2.6$, corresponding to the conventional skin effect. The apparent parameters are $g_{\text{eff}} = 1.92$ and $\Delta B_{\text{pp}} = 202 \pm 8$ mT. Before explaining how we extracted the intrinsic parameters, it is useful to present the ESR spectra obtained after grinding. The X -band spectrum after grinding (Fig. 5, curve *b*) is quite asymmetrical but with $A/B \ll 1$ ($A/B = 0.62$), and the apparent parameters are $g_{\text{eff}} = 2.13 \pm 0.02$ and $\Delta B_{\text{pp}} = 281 \pm 8$ mT. It can be described by considering the presence of the ω_- resonance, and taking

$$y' \propto \frac{U}{(1+U^2)^2} + \frac{V}{(1+V^2)^2} \quad (1)$$

with $V = a(x+1)$. A fit is obtained with $a = 1.16$ and one finally gets $g = 2.037$ and $\Delta B_{i,\text{pp}} = 304 \pm 10$ mT. The Q -band spectrum after grinding (Fig. 6, curve *b*) is symmetrical, and with $g = 2.01$ and $\Delta B_{\text{pp}} = 170 \pm 4$ mT. The Q -band spectrum before grinding (Fig. 6, curve *a*) is well described using a Dysonian shape with $g = 2.013$ and $\Delta B_{i,\text{pp}} = 178 \pm 8$ mT, and an additional linear correction term describing the drift of the base line. It is not possible to describe the line obtained at the X band before grinding using either a Dysonian shape (here A/B is less than 1) or the presence of the wing of the ω_- resonance, or using both. We were able to describe it by considering that we have both the presence of the wing of the ω_- resonance, and a mixture of χ'' and χ' with unequal proportions, which was suggested by the fact that the conventional skin effect does not seem to apply presently.^{7,18} More precisely, we used

$$y' \propto \frac{\alpha - 2U - \alpha U^2}{(1+U^2)^2} - \frac{\alpha + 2V - \alpha V^2}{(1+V^2)^2}, \quad (2)$$

the derivative of

$$y \propto \frac{1 + \alpha U}{1 + U^2} + \frac{1 - \alpha V}{1 + V^2}.$$

For consistency, we used $a = 1.16$, the result found for the X -band spectrum after grinding. The spectrum could be fitted (Fig. 5, curve *a*) with this value and $\alpha = 0.5$, instead of $\alpha = 1$ for a Dysonian line. These values lead to $g = 2.013$ and to the value $\Delta B_{i,\text{pp}} = 307$ mT for the peak-to-peak width of the individual Lorentzian line.

In our first experiments, after grinding of the crystals or sintered samples, the line was still asymmetrical at the Q band. A more efficient grinding led to the present results. The mean diameter of the grains obtained, as measured from electron microscopy, was then $4 \mu\text{m}$. The first results with these fine powders were obtained after dilution into paraffin,¹³ but subsequent measurements showed that the same results were obtained without dilution. In this paper, subsequent results for ground samples are for these fine powders.

From these results and this discussion, it is finally made clear that the ESR spectra can be deeply affected by the skin effect and/or by the presence of the ω_- resonance, however, the results are coherent once these complications are taken into account. It seems reasonable not to treat the different results on an equal footing. The

g value obtained from the ground sample at the Q band seems, for instance, more trustful than the corresponding value before grinding at the X band. Having this point in mind, we conclude, after an examination of the whole of the results, that $g = 2.01 \pm 0.01$ for both the crystals and sintered samples. This should be compared to 1.9925, the free-ion value,¹⁹ and to values found in insulators, for instance, 1.9925 in CaO and 1.991 in CaF₂ and ThO₂.²⁰ $\Delta B_{i,\text{pp}} = 108 \pm 4$ mT at both the X and Q bands, for the crystals, $\Delta B_{i,\text{pp}} = 304 \pm 10$ mT at the X band and 170 ± 4 mT at the Q band for the sintered samples.

What we have called for convenience the intrinsic line does not have in fact, a strictly Lorentzian shape (e.g., Fig. 3, curve *b*), which explains at least partly that, in the presence of the skin effect, the fit with a Dysonian line is not perfect (e.g., Fig. 3, curve *a*). The existence of a (nearly) Lorentzian shape suggests the existence of exchange, which seems more effective in the crystal than in the sintered sample. When going from 9 to 35 GHz, the line is not reduced (crystal from preparation *B*) or reduced only slightly (factor less than 2), which suggests that the $\frac{10}{3}$ effect (cf. Sec. IV) is still effective at 35 GHz.

We now present some ESR results from the crystals obtained with the flux method (preparation *C*), limiting the presentation to the following points: (1) after grinding, the results resemble those from the sintered samples (the apparent values are $A/B \approx 1$, $g_{\text{eff}} = 2.03$, $\Delta B_{\text{pp}} = 158 \pm 4$ mT at the Q band, and $A/B = 0.54$, $g_{\text{eff}} = 2.24$, $\Delta B_{\text{pp}} = 292$ mT at the X band), and (2) before grinding the line is broader than that from the crystals of preparation *B*, and is somewhat anisotropic: at the Q band, $\Delta B_{\text{pp}} = 232$ mT for $c \parallel \mathbf{H}$ and 252 mT for $c \perp \mathbf{H}$, and at the X band $\Delta B_{\text{pp}} = 314$ mT for $c \parallel \mathbf{H}$ and the width varies between 240 and 270 mT when the static field is rotated around the c axis.

We have not been able to establish experimentally how the chemical preparation affects the linewidth. It is natural to imagine that the coupling between Gd^{3+} neighbors could be the superexchange through oxygen ions, and that the occupancy of the oxygen sites could be slightly preparation dependent. In fact, this does not seem to be the case, as can be deduced from ESR observations made after a decrease of the oxygen content by annealing. Figures 7–9 show the 300-K X -band ESR spectra from two samples from preparation *A* (A_1, A_2) and from one sample of type *B*. Figures 7 and 8 are 300-K spectra, while Fig. 9 was obtained at 100 K for a better S/N ratio, the linewidth and shape being the same as at 300 K. Table I gives their T_c before and after annealing (500 °C, air, 10-mm Hg):

We observed that the decrease of the oxygen content, which strongly affects the superconducting behavior, does not change the measured linewidth (at 300 K, 300 mT for A_1 and A_2 , and 110 mT for B_1 , before and after annealing). We also note that even after the annealing of A_2 , which leads to a nonsuperconducting sample, the 300-K ESR line has still a Dysonian shape, which indicates that conduction electrons are still present and mobile at 300 K.

It could perhaps be objected that the whole of the ESR results presented in this paper does not come from the su-

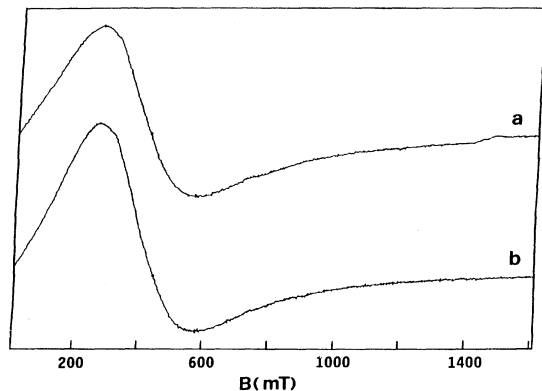


FIG. 7. X-band spectra of the $\text{GdBa}_2\text{Cu}_3\text{O}_{7-\delta}$ A_1 sintered sample at $T=300$ K ($\nu=9388$ MHz, $P=20$ mW, and $B_{\text{mod}}=2$ mT_{pp}). (a) before and (b) after annealing ($T_c \approx 53$ K).

perconducting phase, a situation already found for Cu^{2+} in $\text{YBa}_2\text{Cu}_3\text{O}_7$. It is difficult to eliminate totally this objection only by reasoning, as the reason why Cu^{2+} is ESR silent in $\text{YBa}_2\text{Cu}_3\text{O}_7$ is uncertain. It can, for instance, be argued that the AF couplings between the Gd^{3+} ions are much weaker than between Cu^{2+} , but the absence of the Cu^{2+} signal as a consequence of strong AF coupling is only a suggestion.⁷ We have therefore preferred to check this point directly. Our ESR results upon the starting powder materials (Gd_2O_3 , CuO , BaCO_3) show that an ESR spectrum is found with Gd_2O_3 only. At the X band, the signal from Gd_2O_3 is identical (same shape, ΔB_{pp} and g_{eff} , Fig. 10) to that from a powder of a $\text{GdBa}_2\text{Cu}_3\text{O}_7$ sample of type A . We had, therefore, to clarify this question. We observed that (1) x-ray-diffraction spectra of a $\text{GdBa}_2\text{Cu}_3\text{O}_7$ sample from preparation A do not show the diffraction lines of Gd_2O_3 ; (2) intensity measurements of the X-band ESR line from sample A after grinding and from Gd_2O_3 show that $I(\text{sample } A)/I(\text{Gd}_2\text{O}_3)=0.3$ for the same mass, the ESR signal from sample A cannot originate from Gd_2O_3 as it does not seem realistic to consider that sample A contains 30% (mass proportion) of Gd_2O_3 (sample A is superconducting at 90 K, and does

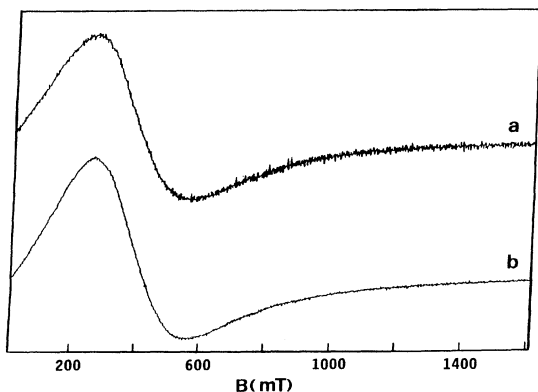


FIG. 8. X-band spectra of the $\text{GdBa}_2\text{Cu}_3\text{O}_{7-\delta}$ A_2 sintered sample at $T=300$ K, with $\nu=9388$ MHz, $P=20$ mW, and $B_{\text{mod}}=2$ mT_{pp}. (a) before and (b) after annealing (not superconducting).

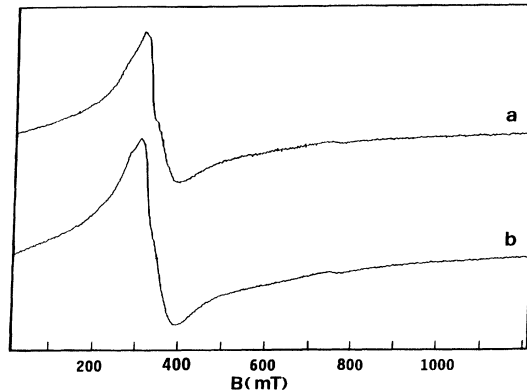


FIG. 9. X-band spectra of the $\text{GdBa}_2\text{Cu}_3\text{O}_{7-\delta}$ single crystal B_1 (mineralization process) at $T=100$ K, with $\nu=9390$ MHz, $P=20$ mW, $B_{\text{mod}}=2$ mT_{pp}, and the static field in the ab plane. (a) before and (b) after annealing ($T_c \approx 52$ K).

not contain the Gd_2O_3 x-ray-diffraction lines); and (3) the ESR line from Gd_2O_3 has the same linewidth at the X and Q bands (280 mT), contrary to what was observed with sample A . One can therefore clearly eliminate the possibility that the ESR line in sample A could originate from Gd_2O_3 .

We therefore finally conclude that the line is due to the Gd^{3+} ions. We will consider that for some still unknown reason the exchange is not fully effective in our sintered samples and in our single crystals prepared by the flux method. This is in agreement with the experimental result that even in the samples prepared by the mineralization process, the linewidth is somewhat sample dependent.¹³ We will keep in mind that when the exchange is fully effective, the width is isotropic and has the same value, 108 ± 4 mT at the X and Q bands. The discussion that follows confirms that the line can be attributed to the Gd^{3+} spins and to their internal couplings.

IV. DISCUSSION

We already know¹³ that if, starting from $\text{GdBa}_2\text{Cu}_3\text{O}_7$, the Gd^{3+} concentration is decreased, the ESR linewidth decreases, indicating that the line in $\text{GdBa}_2\text{Cu}_3\text{O}_7$ is associated with the dipolar coupling. The ESR line shape is not Gaussian but rather Lorentzian, indicating the presence of exchange narrowing. It is helpful to find experimental facts establishing whether the exchange narrowing has its origin in the coupling between the Gd^{3+} ions (Van Vleck-Anderson narrowing mechanism),^{21,22} or between the Gd^{3+} ions and conduction electrons (Plefka-Barnes narrowing mechanism).^{23,24} We found that the

TABLE I: Annealing of samples A_1 , A_2 , B_1 : conditions and effect upon T_c .

	T_c before annealing (K)	Annealing duration	T_c after annealing
A_1	86	1 H	53 K
A_2	86	2 H 40	Not superconducting
B_1	92	2 H 30	52 K

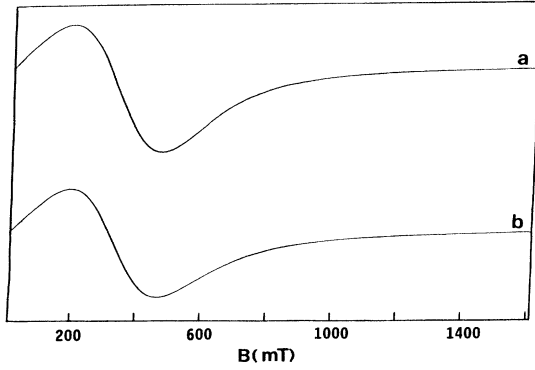


FIG. 10. X-band spectra at $T=300$ K, with $\nu=9382$ MHz, $P=20$ mW, and $B_{\text{mod}}=2$ mT_{pp}. (a) $\text{GdBa}_2\text{Cu}_3\text{O}_7$ A3 sintered sample ($T_c \approx 90$ K) ground and (b) Gd_2O_3 powder.

line shape and width in $\text{GdBa}_2\text{Cu}_3\text{O}_7$ is the same at 150 and 300 K, which shows that the Plefka-Barnes mechanism is presently not operative. If it were, ω_e , the angular frequency for exchange, would be proportional to the inverse of T_{ie} , the relaxation time of the Gd^{3+} spin under the influence of the coupling with the conduction electrons, and we would then have $\omega_e \propto kT$ (Korringa relation²⁵). When lowering the temperature from 300 K, the efficiency of exchange would then decrease and the line would broaden, contrary to what is observed. We will therefore calculate the dipolar width, and the effect of the exchange coupling between the Gd^{3+} ions, for $\text{GdBa}_2\text{Cu}_3\text{O}_7$, both for a powder and, in the case of a single crystal, for several orientations of \mathbf{H} , the static field, using the results of numerical calculations wherever necessary.

We consider that the Gd^{3+} ions are at the nodes of a lattice with tetragonal symmetry with $a=b=c/3$, a realistic model of the situation in $\text{GdBa}_2\text{Cu}_3\text{O}_7$. In the case of a single crystal, we consider \mathbf{H} along c ($\mathbf{H} \parallel [001]$), \mathbf{H} along a ($\mathbf{H} \parallel [100]$), $\mathbf{H} \parallel [110]$, and the case where \mathbf{H} is colinear to the vector with components $a/\sqrt{3}$, $a/\sqrt{3}$, $c/\sqrt{3}$, which we will note $\mathbf{H}:1/\sqrt{3}$. When $\mathbf{H}:1/\sqrt{3}$, the angle between \mathbf{H} and c is roughly 25° .

If the Gd^{3+} ions are coupled by the dipolar coupling but not by exchange (dipolar line), a Gaussian line is expected. For the moment the adiabatic approximation is assumed to be valid, i.e., only that part of the dipolar Hamiltonian which commutes with the Zeeman Hamiltonian, or secular part, is kept in the calculation of M_2 , the second moment of this Gaussian line. Then M_2 has the form

$$\hbar^2 M_2 = \left[\frac{\mu_0 g^2 \beta^2}{4\pi a^3} \right]^2 S(S+1) \Sigma, \quad (3)$$

with

$$\Sigma = \frac{3}{4} \sum_k \frac{(1 - 3 \cos^2 \theta_{k0})^2}{R_{0k}^6}. \quad (4)$$

In the above equations $\sqrt{M_2}$ is expressed in angular frequency units, $R_{0k} = r_{0k}/a$ is the reduced distance between spin k and a spin taken as origin, and θ_{0k} is the an-

gle between the static field and r_{0k} joining these spins. The corresponding width between inflection points is $\Delta B_{\text{pp,dip}} = (1/\gamma) 2\sqrt{M_2}$. In the case of a powder, averaging over the orientations leads to

$$\Delta B_{\text{pp}} = \frac{\mu_0 g \beta}{4\pi a^3} 2 \left[\frac{3}{5} S(S+1) \sum_j \frac{1}{R_{0j}^6} \right]^{1/2}. \quad (5)$$

A numerical calculation gives $\sum_j (1/R_{0j}^6) = 4.7$ (considering the first and second neighbors only gives 4.5). Taking $a = 3.875$ Å (Ref. 14) and $S = 7/2$, one gets $\Delta B_{\text{pp}} = 0.425$ T for a powder. In the case of a single crystal,

$$\Delta B_{\text{pp}} = \frac{\mu_0 g \beta}{4\pi a^3} 2\sqrt{S(S+1)}\sqrt{\Sigma}.$$

Table II gives the values of Σ (numerical determination) and $\Delta B_{\text{pp,dip}}$ for the four selected orientations.

We now examine the influence of exchange upon the ESR linewidth, using the Van Vleck-Anderson-Weiss approach.^{21,22} We call $-2J\mathbf{s}_1 \cdot \mathbf{s}_2$ the exchange coupling between two spins \mathbf{s}_1 and \mathbf{s}_2 . We assume as above the validity of the adiabatic approximation, and compare our theoretical predictions with experiment. $\Delta\omega_{e \cdot n}$, the theoretical width of the exchange-narrowed line in the adiabatic approximation measured between the half-height points of the absorption curve and expressed in angular frequency units, is related to M_2 , and to ω_e , the angular frequency of exchange, through

$$\Delta\omega_{e \cdot n} \simeq \frac{2M_2}{\omega_e} \quad (6)$$

with

$$M'_4 = \frac{\pi}{2} M_2 \omega_e^2. \quad (7)$$

M'_4 is the contribution of exchange to the fourth moment of the ESR line and is given, in the adiabatic approximation, by (cf. the Appendix and Ref. 26)

$$\begin{aligned} \hbar^4 M'_4 = & \left[\frac{\mu_0 g^2 \beta^2}{4\pi a^3} \right]^2 (2J)^2 \\ & \times \left\{ \left[\frac{1}{3} S(S+1) \right]^2 2\Sigma' \right. \\ & \left. + \frac{1}{2} \left[\frac{4}{3} S^2(S+1)^2 - \frac{3}{5} S(S+1) \right] \Sigma'' \right\}. \quad (8) \end{aligned}$$

The expressions for Σ' and Σ'' in (8) are given in the Appendix. In (8) $\hbar(M'_4)^{1/4}$ and J have units of energy, and (8) is established considering that the coupling $2J_{ij}$ is a constant, $2J$, between nearest-neighbor (NN) spins and is zero otherwise, and neglecting terms linear in J against those in J^2 , as initially suggested by Van Vleck. In his

TABLE II. Theoretical dipolar peak-to-peak linewidth for Gd^{3+} in $\text{GdBa}_2\text{Cu}_3\text{O}_7$ (crystal, powder) in the adiabatic approximation.

H	001	100	110	$1/\sqrt{3}$	Powder
Σ	3.54	7.81	1.83	0.44	2.82
$\Delta B_{\text{pp,dip}}$ (T)	0.476	0.708	0.342	0.168	0.425

explicit computation of the fourth moment for a simple-cubic lattice (distance between NN = d), Van Vleck moreover neglected dipolar terms connecting atoms separated by distances greater than $2d$, and neglected the Σ'' term, noticing that its spin-dependent factor is zero if $S = \frac{1}{2}$. We did a numerical calculation of M'_4 without these last two simplifications [use of numerical methods makes the first one unnecessary, and the validity of the second one is uncertain in the present case ($S = \frac{7}{2}$)]. The predicted value of the exchange-narrowed linewidth for the powder, and for the chosen orientations of the static magnetic field in the case of a single crystal, are collected in Table III, taking the width for $\mathbf{H} \parallel c$ as a reference.

The theoretical widths for the powder and for $\mathbf{H} \parallel c$ are significantly different, and moreover a strong anisotropy in the ab plane is predicted, and the width for the three orientations in that plane should differ strongly from that when $\mathbf{H} \parallel c$. In fact, the experimental width is isotropic. This discrepancy between experimental and theoretical results suggests that our initial assumption—adiabatic approximation—is presently invalid. Both the secular and the nonsecular parts of the dipolar Hamiltonian should be considered. Then the theoretical line is isotropic, the second moment is $\frac{10}{3}$ times its value calculated for a powder in the adiabatic approximation, and this is equally true for the part of the fourth moment associated with exchange²⁷ ($\frac{10}{3}$ effect^{21,22}). The results in Ref. 27 have been established for cubic symmetry. We will consider that they constitute a first approximation in the present case with tetragonal symmetry, without being able to totally exclude the possibility for the Gd^{3+} ions of occupying not the Y^{3+} sites, as generally thought, but the nodes of a lattice with cubic symmetry. Equation (6) is then still valid, but with the modified M_2 value and can be used to determine ω_e through

$$\frac{\omega_e}{\gamma} = \frac{1}{2\sqrt{3}} \frac{(\Delta B'_{\text{pp,dip}})^2}{\Delta B_{\text{pp,expt}}}, \quad (9)$$

where $\Delta B_{\text{pp,expt}}$ is the peak-to-peak width of the experimental (Lorentzian) line, and $(\Delta B'_{\text{pp,dip}})^2$ is $\frac{10}{3}$ times the square of the peak-to-peak width of the (Gaussian) dipolar line calculated for a powder within the adiabatic approximation. We have found that $\Delta B_{\text{pp,expt}} = 0.108$ T. Therefore,

$$\frac{\omega_e}{\gamma} = \frac{1}{2\sqrt{3}} \left[\frac{10}{3} \right] \frac{0.425^2}{0.108} = 1.61 \text{ T}.$$

This value should be compared to the Zeeman angular frequency ω_z (at the Q band $\omega_z/\gamma = 1.25$ T). This means that even at the Q band $\omega_e \gtrsim \omega_z$. Consequently, even at

TABLE III. Theoretical value of the exchange-narrowed line, in the adiabatic approximation, taking the value for $\mathbf{H} \parallel c$ as a reference.

H orientation	001	100	110	$1/\sqrt{3}$	Powder
Theoretical exchange-narrowed line	1	2.12	0.46	0.11	0.76

the Q band the adiabatic approximation is expected to be invalid. It is equivalent to say that the nonsecular part of the dipolar Hamiltonian should manifest itself as a cause of broadening at the X band ($\frac{10}{3}$ effect) and should be as effective at the Q band. We did observe experimentally that the linewidth was the same at 35 GHz as at 9 GHz. We also observed that for the samples where the exchange is less effective, i.e., ω_e smaller (sintered samples and crystals prepared by the flux method), the line was narrower at the Q band, the difference being less than $\frac{10}{3}$, which is in agreement with our interpretation.

We are now in a position to calculate $2J$, the coupling constant between two NN Gd^{3+} spins, using our experimental results and the results of this analysis. Using Eq. (7) and the expression for M'_4 and M_2 valid in the nonadiabatic case, namely [Eq. (A5) and Table V of the Appendix, and Eq. (3) and Table II]

$$\hbar^4 M'_4 = \left[\frac{\mu_0}{4\pi} \cdot \frac{g^2 \beta^2}{a^3} \right]^2 (2J)^2 2825 \left(\frac{10}{3} \right), \quad (10)$$

$$\hbar^2 M_2 = \left[\frac{\mu_0}{4\pi} \cdot \frac{g^2 \beta^2}{a^3} \right]^2 S(S+1) 2.82 \left(\frac{10}{3} \right), \quad (11)$$

one finally gets

$$2J/k = \left[\frac{\pi}{2} S(S+1) \frac{2.82}{2825} \right]^{1/2} \frac{\hbar \omega_e}{k} = 0.33 \text{ K}. \quad (12)$$

Before discussing this result, we note that our calculations (see the Appendix) show that neglecting the second term of M'_4 finally constitutes a reasonable approximation even in the present case of an $S = \frac{7}{2}$ spin, which was initially uncertain. We also note that replacing Eq. (8) (with the addition of the $\frac{10}{3}$ factor) by the approximate expression

$$\hbar^4 M'_4 \simeq \left[\frac{\mu_0}{4\pi} \cdot \frac{g^2 \beta^2}{a^3} \right]^2 (2J)^2 \left[\frac{1}{3} S(S+1) \right]^2 77.8 \left(\frac{10}{3} \right) \quad (13)$$

and using Eqs. (7), (11), and (13), one gets $\omega_e^2 \simeq 1.95(2J/\hbar)^2 S(S+1)$; in the case of a simple-cubic lattice and with the same approximation, one would get a result of similar form, with 2.8 instead of 1.95.²⁶ We finally compare our result for $2J/k$ with that deduced from the knowledge of the transition temperature T_N . It is well known that the expression deduced from the molecular field model, $2J/k = 3T_N/zS(S+1)$ (z is the number of NN of a given spin) is only a poor approximation of reality. The more exact calculation by Rushbrooke and Wood gives $2J/k = 1.79[3T_N/zS(S+1)]$ for a simple-cubic lattice and $S = \frac{1}{2}$.²⁸ Accepting this result for the present case ($S = \frac{7}{2}$), one gets $J/k = 0.2$ K [$T_N = 2.24$ K (Ref. 29)]. The difference between this value and our result from ESR is not surprising, due to the assumptions made in both approaches. On the contrary, we think that the whole of our results clearly confirms that the 300-K ESR spectrum observed in $\text{GdBa}_2\text{Cu}_3\text{O}_7$ does come from the Gd^{3+} spins and their internal couplings, and that it is possible to neglect their coupling with the spin of either the Cu^{2+} ions or the conduction electrons at this level of approximation.

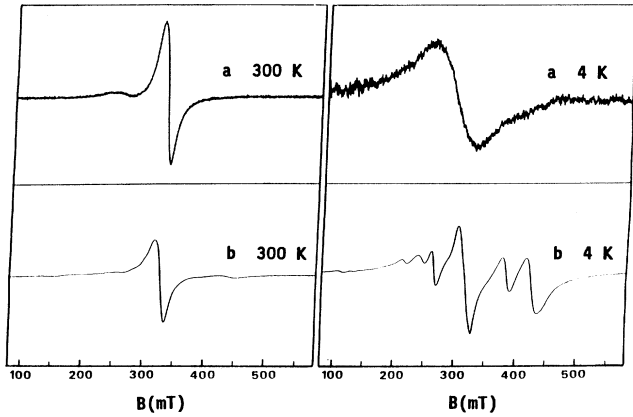


FIG. 11. X-band spectra for a $\text{Y}_{0.98}\text{Gd}_{0.02}\text{Ba}_2\text{Cu}_3\text{O}_{7-\delta}$ single crystal prepared by the mineralization method. $\nu = 9388$ MHz, $P = 20$ mW, and $B_{\text{mod}} = 2$ mT_{pp}. The spectra have been recorded. (a) before annealing ($T_c \simeq 90$ K), at 300 K (curve a, 300 K) and at 4 K (curve a, 4 K); and (b) after annealing (superconductivity has been suppressed, see caption Fig. 12), at 300 K (curve b, 300 K) and at 4 K (curve b, 4 K).

V. CONCLUSION

Based on experimental and theoretical results, the following picture finally emerges: in $\text{GdBa}_2\text{Cu}_3\text{O}_7$ one can consider two distinct systems, the Gd^{3+} ions and the conduction electrons. The Gd^{3+} ions are coupled by both the dipolar and the antiferromagnetic exchange couplings. The efficiency of the dipolar coupling is reduced by the AF coupling, which at the ESR scale appears as a narrowing of the ESR dipolar line. The exchange constant between NN deduced from ESR spectra is $2J/k = -0.33$ K. The exchange coupling between the Gd^{3+} spins and the conduction electrons is weaker than between Gd^{3+} spins and has no effect upon the width of the ESR line at 300 K. It is tempting to suppose, however, that this coupling is responsible for (1) the small g shift observed in ESR (Hasegawa mechanism²⁵) and (2) the difficulty to observe a well-resolved fine structure in $\text{Y}_{1-x}\text{Gd}_x\text{Ba}_2\text{Cu}_3\text{O}_7$ with low Gd^{3+} concentration at 300 K.¹³ Before concluding, we have tried to check one of these suggestions experimentally. The g shift is small, and we therefore preferred to test the question of the fine structure. We recorded the X-band ESR spectrum from a single crystal with $x = 2\%$ Gd, at both 300 and 4 K, before and after annealing. In our interpretation, before annealing, at this concentration the 300-K spectrum (Fig. 11, curve a 300 K) is exchange narrowed by the Plefka-Barnes mechanism, and the fine structure is unobserved. We will discuss the effect of the passage through T_c in

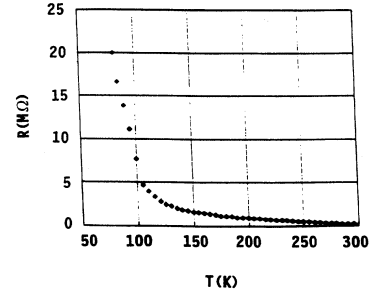


FIG. 12. Thermal dependence of the resistance of the $\text{Y}_{0.98}\text{Gd}_{0.02}\text{Ba}_2\text{Cu}_3\text{O}_{7-\delta}$ crystal used in Fig. 11, after 17-h annealing at 800°C , in a 2.5-mm Hg N_2 atmosphere. After this annealing the sample was not superconducting even at 4 K.

both the $x = 1$ and dilute samples separately, and here we just present the ESR spectrum recorded at 4 K in this superconducting material (Fig. 11, curve a, 4 K). After annealing, the material is no longer superconducting. At 300 K, conduction electrons are, however, still present and mobile (see Sec. III). When the temperature is decreased, the resistivity increases strongly (Fig. 12), and at a low enough temperature the concentration of the carriers can be expected to be low enough for the exchange coupling to become inefficient. Exchange narrowing will then be absent and the fine structure will be observable. The fine structure in the $\text{Y}_{0.98}\text{Gd}_{0.02}\text{Ba}_2\text{Cu}_3\text{O}_7$ annealed sample did appear in a spectacular manner below roughly 100 K. Figure 11, curve b, 4 K shows the spectrum recorded at $T \simeq 4$ K. From the general discussion of our experimental results, we will also keep the idea that additional experiments seem of interest, in order to measure the T_N value in $\text{GdBa}_2\text{Cu}_3\text{O}_7$ samples from both preparations A and B, to check the positions of the Gd^{3+} ions, and to study more systematically the ESR in samples with partial gadolinium substitution.

ACKNOWLEDGMENTS

We wish to thank J. B. Faure for his technical assistance, and Dr. P. Monod for his remarks concerning a preliminary version of this work. We also thank Dr. A. Stepanov (Institute for Low Temperature Physics and Engineering, Kharkov, Ukraine), present in our lab during the very end of this work, for interesting comments. Financial support was provided by CNRS.

APPENDIX: CALCULATION OF M'_4

We write $-2J\mathbf{s}_i \cdot \mathbf{s}_j$, the exchange coupling between two spins, as in Ref. 28 (see Sec. IV). The starting expression for M'_4 , where $(\hbar^4 M'_4)^{1/4}$ has units of energy, is

$$\hbar^4 M'_4 = \left[\frac{\mu_0}{4\pi} g^2 \beta^2 \right]^2 N^{-1} \left\{ \sum_{j,k,l \neq} [2(2J)_{jk}^2 (b_{jl} - b_{kl})^2 + 2(2J)_{jk}(2J)_{kl}(b_{jl} - b_{jk})(b_{jl} - b_{kl})] \right. \\ \left. \times \left[\frac{1}{3} S(S+1) \right]^2 + \sum_{k>j} b_{jk}^2 (2J)_{jk}^2 \left[\frac{4}{5} S^2(S+1)^2 - \frac{3}{5} S(S+1) \right] \right\}, \quad (\text{A1})$$

TABLE IV. The values of the dimensionless sums Σ' and Σ'' for a powder and for selected orientations of the field for spins at the nodes of a lattice with tetragonal symmetry.

H	001	100	110	$1/\sqrt{3}$	Powder
Σ'	42.73	99.97	34.03	10.03	38.91
Σ''	9.0	22.5	2.25	0	7.2

where $b_{jk} = \frac{3}{2}[(1 - 3 \cos^2 \theta)/r_{jk}^3]$. This expression for M'_4 is equivalent to Van Vleck's results.²¹ In the expression for M'_4 , the terms linear in the exchange coupling are far smaller than the quadratic terms and have been neglected. N is the number of spins, the sum $\sum_{j,k,l \neq}$ means that the three indices j, k, l must be different. Taking $J_{ab} = J$ if a and b are nearest neighbors and $J_{ab} = 0$ otherwise, then

$$\hbar^4 M'_4 = \left[\frac{\mu_0}{4\pi} g^2 \beta^2 \right]^2 (2J)^2 \times \left\{ \left[\frac{1}{3} S(S+1) \right]^2 2\Sigma_1 + \frac{1}{2} \left[\frac{4}{5} S^2(S+1)^2 - \frac{3}{5} S(S+1) \right] \Sigma_2 \right\}. \quad (\text{A2})$$

In this expression

$$\Sigma_1 = \sum_{j,l} 2(b_{jl}^2 - b_{jl}b_{ol}) + \sum_{j,l} [b_{jl}^2 - 2b_{ol}b_{jl} + b_{ol}b_{ol}], \quad (\text{A3})$$

TABLE V. M'_4 , the exchange contribution to the fourth moment of the ESR line (first and second terms, and their sum).

H	001	100	110	$1/\sqrt{3}$	Powder
$\frac{441}{8} \Sigma'$	2355	5511	1876	553	2145
$94.5 \Sigma''$	851	2126	213	0	680
Total	3206	7637	2089	553	2825

and

$$\Sigma_2 = \sum_j b_{0j}^2. \quad (\text{A4})$$

In the expressions for Σ_1 and Σ_2 , a spin (spin 0) is taken as origin, j is a NN of 0. In the expression for Σ_1 , l is distinct from 0 and j , and is otherwise arbitrary for the two first terms, while it is a NN of 0 for the three remaining terms. Concerning the case of identical spins at the nodes of a lattice with tetragonal symmetry ($\alpha = \beta = \gamma = \pi/2$) and $a = b = c/3$, we have calculated the dimensionless sums $\Sigma' = a^6 \Sigma_1$ and $\Sigma'' = a^6 \Sigma_2$ for a powder and for the three chosen orientations of \mathbf{H} in the case of a single crystal. The "spin-independent" results for Σ' and Σ'' are given in Table IV.

When $S = \frac{7}{2}$, Eq. (A2) gives

$$\hbar^4 M'_4 = \left[\frac{\mu_0}{4\pi} \frac{g^2 \beta^2}{a^3} \right]^2 (2J)^2 \left[\frac{441}{8} \Sigma' + 94.5 \Sigma'' \right]. \quad (\text{A5})$$

The two contributions to M'_4 are given separately in Table V.

¹P. G. De Gennes, C. R. Acad. Sci. (Paris) **305**, 345 (1987).

²P. W. Anderson, Science **235**, 1196 (1987).

³E. Sigmund and K. W. H. Stevens, J. Phys. C **63**, 6025 (1987).

⁴D. C. Vier, S. B. Oseroff, C. T. Salling, J. F. Smyth, S. Schultz, Y. Dalichaouch, B. W. Lee, M. B. Maple, Z. Fisk, and J. D. Thomson, Phys. Rev. B **36**, 8888 (1987).

⁵A. Deville, B. Gaillard, H. Noel, M. Potel, P. Gougeon, and J. C. Levet, International Conference on High Temperature Superconductors, Materials and Mechanisms of Superconductivity, Interlaken, 1988 [Physica C **153-155**, 669 (1988)].

⁶J. Albino, O. De Aguiar, A. A. Menovsky, J. Van Den Berg, and H. B. Brom, International Conference on High Temperature Superconductors (Ref. 5), p. 743.

⁷A. Deville, B. Gaillard, H. Noel, M. Potel, P. Gougeon, and J. C. Levet, J. Phys. (Paris) **50**, 2357 (1989).

⁸A. A. Abrikosov and L. P. Gor'kov, Zh. Eksp. Teor. Fiz. **39**, 1781 (1960) [Sov. Phys. JETP **12**, 1243 (1961)].

⁹R. N. Schwartz, A. C. Pastor, R. C. Pastor, K. W. Kirby, and D. Rytz, Phys. Rev. B **36**, 8858 (1987).

¹⁰F. Nakamura, K. Senoh, T. Tamura, Y. Ochiai, and Y. Narahara, Phys. Rev. B **39**, 12 283 (1989).

¹¹H. Kikuchi, Y. Ajiro, Y. Ueda, K. Kosuge, M. Takano, Y. Takeda, and M. Sato, J. Phys. Soc. Jpn. **57**, 1887 (1988).

¹²F. Mehran, S. E. Barnes, C. C. Tsuei, and T. R. McGuire, Phys. Rev. B **36**, 7266 (1987).

¹³A. Deville, B. Gaillard, L. Bejjit, O. Monnereau, H. Noel and M. Potel, Physica B **165-166**, 1319 (1990).

¹⁴R. Beyers and T. M. Shaw, in *Solid State Physics*, edited by H. Ehrenreich and D. Turnbull (Academic, London, 1989), Vol.

42.

¹⁵S. A. Hodorowicz, A. Chodorowicz-Bak, J. Czerwonka, E. Hodorowicz, W. Lasocha, and H. A. Eick, J. Solid State Chem. **92**, 480 (1991).

¹⁶T. S. Al'tshuler, I. A. Garifullin, and E. G. Kharakhash'yan, Fiz. Tverd. Tela (Leningrad) **14**, 263 (1972) [Sov. Phys. Solid State **14**, 213 (1972)].

¹⁷C. Rettori, D. Davidov, P. Chaikin, and R. Orbach, Phys. Rev. Lett. **30**, 437 (1973).

¹⁸A. Deville, H. Fawaz, B. Gaillard, H. Noel, M. Potel, and O. Monnereau, Mater. Sci. Eng. B **14**, 175 (1992).

¹⁹R. Lacroix, Helv. Phys. Acta **30**, 374 (1957).

²⁰A. Abragam and B. Bleaney, *Résonance Paramagnétique Electronique des Ions de Transition* (PUF, Paris, 1971).

²¹J. H. Van Vleck, Phys. Rev. **74**, 1168 (1948).

²²P. W. Anderson and P. R. Weiss, Rev. Mod. Phys. **25**, 269 (1953).

²³T. Plefka, Phys. Status Solidi B **51**, K113 (1972); **55**, 129 (1973).

²⁴S. E. Barnes, Phys. Rev. B **9**, 4789 (1974); J. Phys. F **4**, 1535 (1974); **6**, 1713 (1976).

²⁵H. Hasegawa, Prog. Theor. Phys. **21**, 483 (1959).

²⁶A. Abragam, *Les Principes du Magnétisme Nucléaire* (PUF, Paris, 1961).

²⁷B. R. Cooper and F. Keffer, Phys. Rev. **25**, 896 (1962).

²⁸C. Kittel, *Physique de l'Etat Solide* (Dunod, Paris, 1983).

²⁹B. D. Dunlap, M. Slaski, Z. Sungaila, D. G. Hinks, K. Zhang, C. Segre, S. K. Malik, and E. E. Alp, Phys. Rev. B **37**, 592 (1988).